Plasma Phys. Control. Fusion **41** (1999) 867–879. Printed in the UK PII: S0741-3335(99)01102-1

Spectroscopic evidence for high harmonic fast wave heating in the CDX-U spherical torus

D Stutman†, M Finkenthal†, V Soukhanovskii†, J Menard‡, T Munsat‡, R Kaita‡ and R Majeski‡

† Johns Hopkins University, Baltimore, MD 21218, USA
‡ Princeton Plasma Physics Laboratory, Princeton University, Princeton, NJ 08543, USA

Received 20 January 1999, in final form 27 April 1999

Abstract. We present evidence for high harmonic fast wave (HHFW) heating in the core of the CDX-U spherical torus (aspect ratio $R/a \approx 1.5$) at the Princeton Plasma Physics Laboratory. We use a spectroscopic technique combining fast, multichordal measurements of the ultrasoft x-ray line emission from intrinsic C and O. The results show that in a few cases substantial (nearly 50%) increases in the core electron temperature can be obtained with only about 100 kW of radio-frequency power, compared to ≈150 kW ohmic input. Modifications of the core magnetohydrodynamic activity consistent with the estimated T_e increase are also observed. The majority of the discharges exhibit only modest core T_e increases however, with most of the heating occurring outside $r/a \approx 0.5$. A proposed explanation for this effect consistent with the experimental observations is based on a neoclassical transport instability for low-Z impurities, similar to an effect recently described for high-Z impurities in large tokamaks.

1. Introduction

Spherical tori (ST) having aspect ratio $A \equiv R/a \leqslant 1.5$ have been investigated as a cost effective alternative to the tokamak fusion concept [1]. The attractiveness of the ST arises from its compactness and the possibility of achieving high plasma pressure with low magnetic field (high β). Efficient coupling of radio-frequency (RF) waves to the plasma is critical for the success of ST due to the inherent limitation in the start-up and heating capability of an ohmic transformer in the tight aspect ratio ST configuration. High harmonic fast waves (HHFW) are predicted to be an efficient tool for plasma heating and current drive in the high β, ST plasma [2].

The CDX-U spherical torus at the Princeton Plasma Physics Laboratory is the first device to experimentally investigate the physics of HHFW coupling and heating in the ST geometry, using a 12 MHz system equipped with a rotatable antenna, and typically delivering up to ≈100 kW for several ms [3]. The typical CDX-U parameters are: $R \approx 35$ cm, $a \approx 23$ cm, $A \approx 1.5$, elongation ≈1.5, toroidal field $B_{TO} \approx 0.12$ T and ohmic heating power ≈150–200 kW. It routinely achieves $I_p \approx 60$–75 kA at an effective safety factor $q_{cyl} \approx 2$, with plasma duration around 20 ms and a few ms 'flat-top'. The typical ohmic plasma has central electron temperature $T_{e0} \approx 80$–100 eV and line-averaged electron density $\int n_e \, dL/L$, around 6–8×10^{18} m^{-3}. The discharge is characterized by persistent magnetohydrodynamic (MHD) activity, manifested as a system of permanently coupled, $m = 1/n = 1$ ('snake') and $m = 2/n = 1$ islands [4].

0741-3335/99/070867+13$30.00

The main diagnostic in this work is a high spatial resolution (≈0.8 cm at plasma axis) array of surface barrier diodes, having 33 active chords staggered in a (3 × 11) matrix and covering mainly the plasma inside the $q = 1$ surface at $r/a \approx 0.5$. The array is filtered with a thin (0.3 μm) Ti foil, which efficiently transmits in the 30–60 Å band, while completely rejecting light above ≈100 Å. Extensive spectroscopic investigations show that in CDX-U conditions the array predominantly measures the C V $1s^2$–1snp resonance emission (dominated by the intense $1s^2$–1s2p lines around 40.5 Å) [5, 6].

Another relevant diagnostic is a multilayer mirror/photodiode monochromator which measures with a few angström spectral resolution the O VI 2s–3p lines around 150 Å, and views the same chord as the central diode in the array [6, 7]. In addition, an absolute photodiode is used to estimate the radiated power losses from the plasma [8, 9], while a visible monochromator monitors lines of edge impurity ions (typically, O II or C III).

The line-integrated electron density is monitored with a 2 mm microwave interferometer which vertically views the plasma. A multipass/multipulse Thomson scattering system measuring the central electron temperature with ≈10% accuracy was available for part of the measurements [10]. Finally, a triple Langmuir probe is used for measurements of the electron temperature and density profile evolution outside the core ($r/a > 0.65$) [3].

2. Results

Figure 1 presents the traces of the line-integrated electron density and spectroscopic signals for successive ohmic (OH) and auxiliary heated (RF) discharges. The plasma current signal was affected by pick-up during the RF pulse and is not shown. The spectroscopic signals are

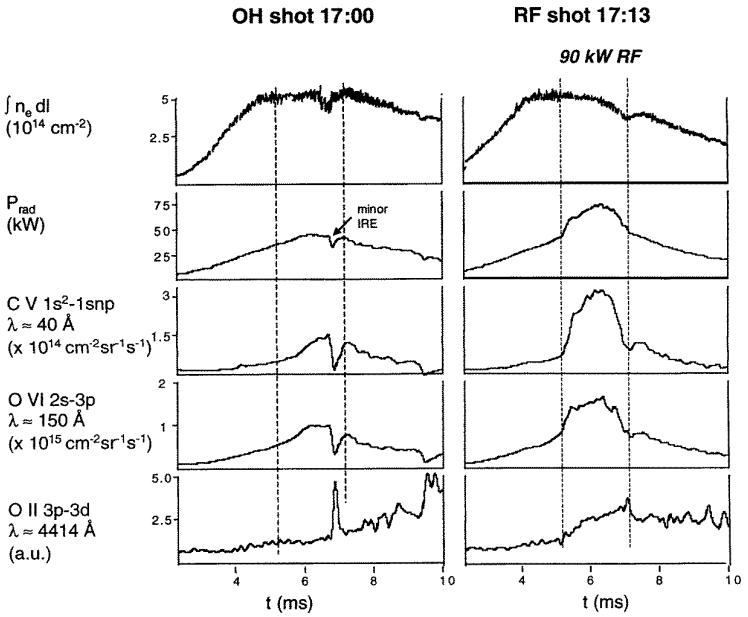

Figure 1. Electron density and spectroscopic traces in successive ohmic and auxiliary heated discharges.

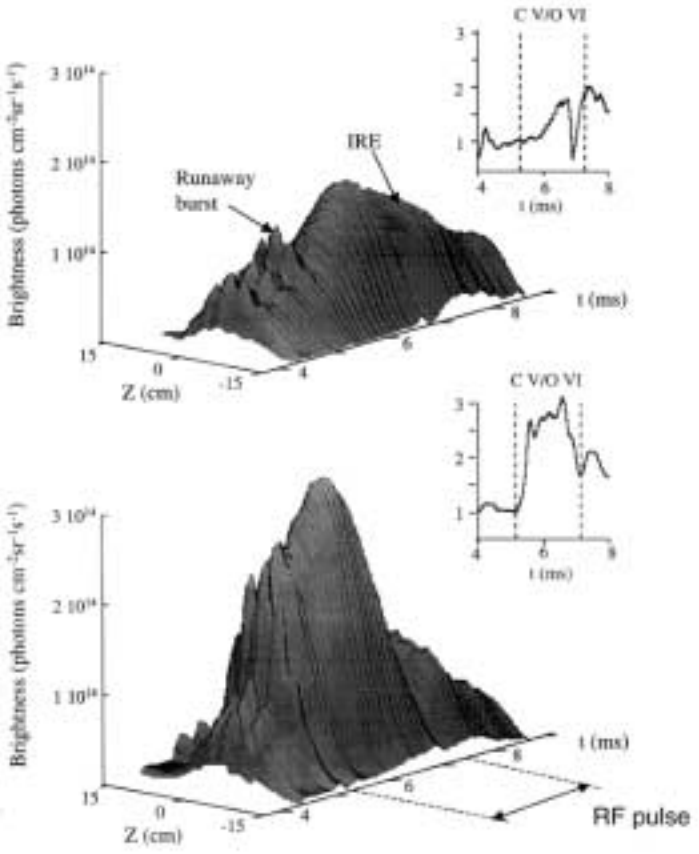

Figure 2. C v emission profile evolution in the OH and RF discharges. The signals are low-pass filtered at 5 kHz to remove the MHD fluctuations. The spikes apparent at earlier times are caused by bursts of runaways hitting the inside limiter. (The spikes appear in every third channel because only one column of diodes out of three sees the limiter.)

low-pass filtered at ≈5 kHz to remove the large 10 kHz fluctuations associated with the $m = 1$ 'snake'. A 'flat-top' of ≈2 ms is apparent on the density trace in both discharges. No density increase is evident during the RF pulse, indicating that the impurity influx due to the pulse is small.

The sudden drop in the C v emission occurring in both discharges around $t \approx 7$ ms is the signature of a (mild) internal reconnection event (IRE). This is a global MHD event resembling the minor disruption in conventional tokamaks and has been observed in several other ST devices [11]. Prior to the IRE, the spectroscopic signals show a large and steep increase in the C v emission during the RF pulse, accompanied by a less prominent rise in the O vi signal. A relatively modest increase in the radiated power is estimated using the diode bolometer. This is typical of well conditioned discharges; in less clean plasmas we observe a significant fraction of the input power being radiated away, as well as an electron density increase during the RF pulse. The O ii emission at the plasma edge also slowly increases, possibly indicating some additional impurity influx during the RF pulse. We note, however, that this line is not a faithful

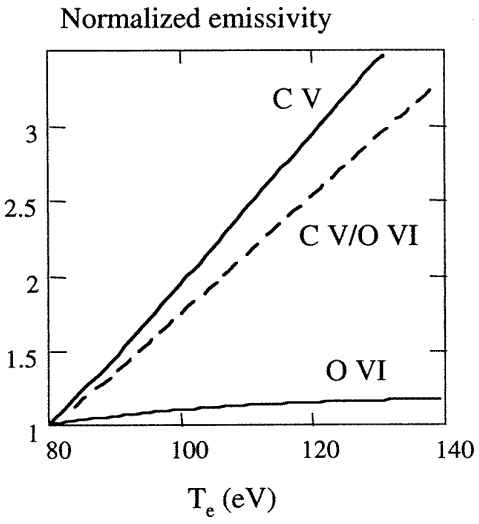

Figure 3. Computed emissivity of the C v 40.5 Å and O vi 150 Å resonance transitions as a function of T_e, relative to the 80 eV value (the typical CDX-U core temperature).

influx monitor. Due its relatively high excitation energy ($\Delta E \approx 23$ eV) it also reflects an edge temperature increase, which is quite routinely observed during RF discharges [3].

The C v emission profile evolution in figure 2 shows that the fast increase observed during the RF pulse is strongly peaked in the core. Milder peaking is nevertheless also seen in the ohmic only discharge, although at later times. The flattening of the emission at the IRE reflects a similar change in the temperature profile [11].

The differences between the two discharges are most evident in the evolution of the ratio between the central C v and O vi intensities, normalized to the pre-RF value (briefly, the C v/O vi ratio). During the RF pulse it abruptly increases, whereas in the OH discharge it stays nearly constant between 5 and 6 ms.

One explanation for these observations would be a rapid and significant increase in the core temperature during the RF pulse. Indeed, for typical CDX-U core temperatures, the C v line ($\Delta E \approx 306$ eV) is a very sensitive indicator of temperature changes, whereas the O vi line ($\Delta E \approx 82$ eV) is practically unaffected (figure 3). (Similarly a milder temperature increase occurs later in the OH discharge, while the post-IRE evolution indicates a recovery of the core temperature.) This interpretation presupposes that: (i) both C v and O vi emit from the core region; (ii) the *relative* influx increases during the RF pulse (if any) are the same for C and O; and (iii) the changes in the ionization balance are negligible.

Tangential scans with a high-resolution spectrometer show that the O vi emissivity is indeed peaked on the discharge axis. Moreover, O v is also present inside the $q = 1$ radius. Another indication that both C v and O vi emit from this region comes from the fact that their signals exhibit the MHD modulation characteristic of the $m = 1$ 'snake' [6]. As discussed later, the presence of O v and O vi in the CDX-U core is the consequence of fast radial transport.

Concerning the second assumption, a direct measurement of the impurity influx is difficult. At the low particle energies encountered in CDX-U we expect the main source of O and C impurities to be the weakly bound atoms on the vacuum chamber and not localized sputtering sources, which might preferentially increase the influx of one species. In any case, as shown

later, this assumption is indirectly verified by measurements and supported by the modelling results.

Addressing the third assumption, the changes in the ionization balance still need to be taken into account, however. This is evident, for example, from the O VI increase after $t \approx 6$ ms in the ohmic discharge (figure 1). In the absence of any change in the edge emission, the core emission increase indicates an accelerated 'burn-through' of the lower oxygen charge states. To account for the ionization dynamics and impurity transport we modelled the emission data using the measured plasma profile data and the time-dependent, multiple ionization state transport (MIST) code [12]. The ohmic plasma was modelled as follows.

Estimated electron density and temperature profiles. The density profile is obtained by fitting the Langmuir probe results for $r/a > 0.65$ [3], and using the $\int n_e \, dL$ interferometer data to constrain the density inside this region. The result is a strongly peaked profile, with most of the density concentrated inside the $q = 1$ surface. The initial guess for the fit of the temperature profile is obtained by matching the Langmuir probe data to the central Thomson scattering value, T_{e0}. The time evolution of T_{e0} is measured by a shot-to-shot temporal scan.

Impurity transport. The available data does not allow a detailed evaluation of the CDX-U transport. However, an estimate of the rate of change in the impurity density n_I, in the core is sufficient for an assessment of the heating effect. We assume a constant diffusion coefficient $D_\perp$, to quantify this rate

$$-D_\perp \frac{\partial n_I}{\partial r} \approx -\frac{\partial}{\partial t}\left[\frac{1}{r}\int_0^r n_I r' \, dr'\right]. \tag{1}$$

A convective velocity term describing the degree of peaking of the impurity profile may also be present in (1). Although this term cannot be estimated from the available data, the heating result does not significantly depend on the details of the impurity distribution in the CDX-U core.

A lower limit for $D_\perp$ is given by the neoclassical value. Collisionality estimates using Artsimovich scaling for the ion temperature [13] show that in CDX-U both C V and O VI are well into the Pfirsch–Schluter regime. Using the neoclassical result from [14], we arrive at a diffusion coefficient $D_{neo}^{PS} \approx 15$–20 m^2 s^{-1}. This large value is a consequence of the low toroidal field (the typical impurity ion Larmor radius is nearly 1 cm) and high collisionality.

However, we are more interested in an upper limit. Indeed, slower transport would only prolong the time scales for impurity penetration, adding support to the heating interpretation of the observed fast emission increases. This estimate is based on RF discharges in which there are no indications of core heating, but which show a large and gradual ($\approx$1.5 ms rise time) increase in all the spectroscopic signals following the RF pulse; this increase can be primarily attributed to a transient impurity influx. The rise time can be modelled using a diffusion coefficient around 40 m^2 s^{-1}. Transport of this magnitude is also needed in order to reproduce the presence of O V inside $r/a \approx 0.5$. Very similar values are reported from other low-field devices [15].

Impurity source. The neutral source is estimated by matching the experimental C V and O VI brightness values. This procedure also satisfactorily reproduces the time history of edge emission. The estimated average concentrations are relatively high, around 3–3.5% for both carbon and oxygen.

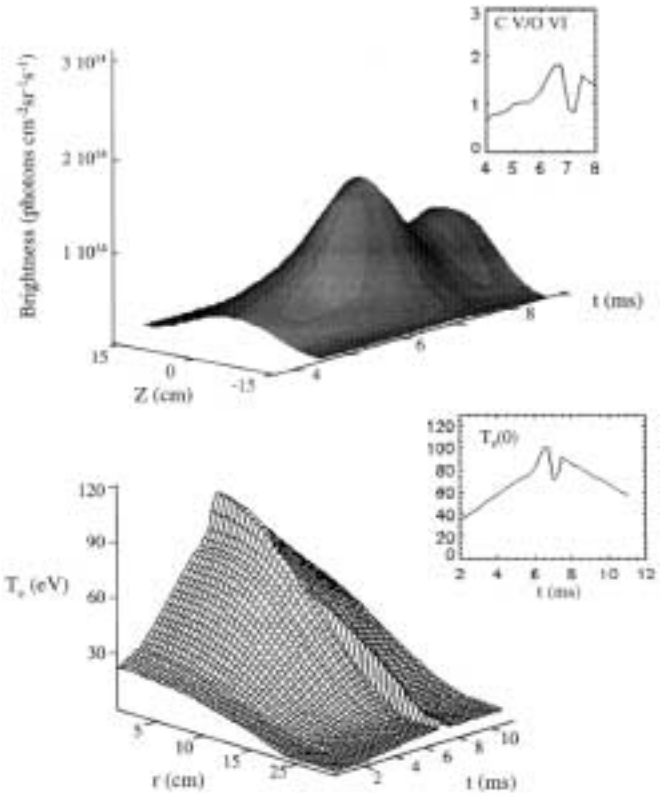

Figure 4. Computed spectroscopic signals and the temperature distribution for the ohmic discharge.

Charge exchange recombination. To account for charge exchange (CX) recombination we assumed a neutral hydrogen background density typical for small tokamaks $N_{\mathrm{H}} \approx 0.1 \times N_{\mathrm{e\,SOL}}$ [16]. With this assumption the CX effect is significant only during the lower density stage of the discharge. The measurement of the H_α line indicates that the neutral density does not significantly increase during the RF pulse.

Using these assumptions, $T_{\mathrm{e}}(r, t)$ for the ohmic discharge is then obtained by modifying the T_{e} profile, while keeping fixed the rest of the plasma parameters, until the measured and computed C V distributions are matched. The procedure is robust, due to the strong sensitivity (approximately $\sim T_{\mathrm{e}}^{2.7\text{–}2.8}$) of the C V emission map on T_{e}. An elongation of $\approx$1.5 inferred from equilibrium computations [3] is used to transform the MIST profiles into two-dimensional (2D) emissivity maps, which are then integrated along the array chords. For completeness, we also roughly modelled the IRE as a drop and flattening of the T_{e} profile [11].

The results indicate a temperature profile evolving from slightly hollow to peaked, within $\approx$1.5 ms before the IRE. The computed C V emission profiles are in fair agreement with the experiment, while the central chord C and O signals and their ratio are also quite well reproduced (figure 4). The O VI increase is indeed predicted as an accelerated 'burn-through' of the lower charge states.

The auxiliary heated case is modelled as follows. Prior to the RF pulse we assume the same plasma parameters as for the OH discharge. This is justified by the similar evolution of

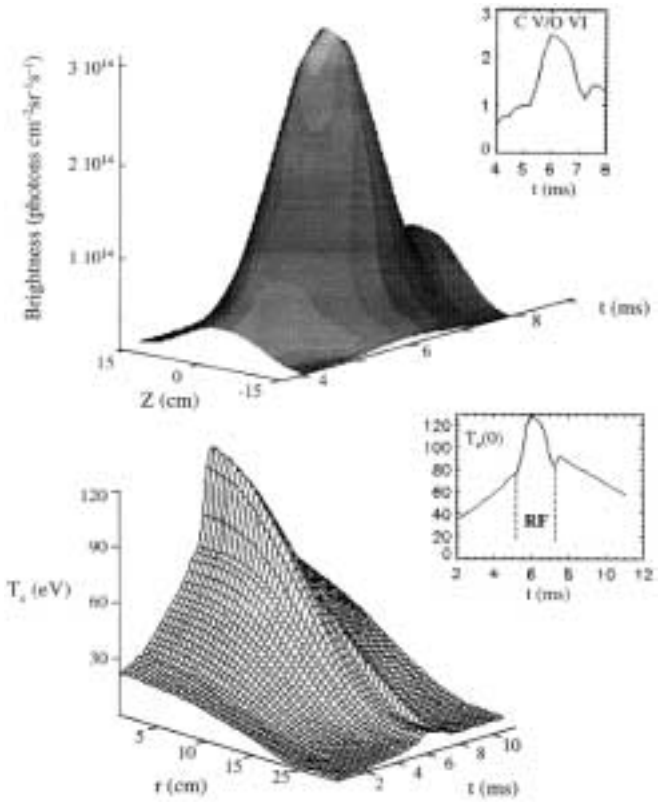

Figure 5. Computed signals and the estimated temperature evolution for the RF discharge.

the line-integrated electron density and of all the spectroscopic signals. The RF pulse is then modelled assuming that the density is unchanged (as suggested by the traces of figure 1), but that a temperature increase $\Delta T_{\mathrm{e\,RF}}$, as well as an impurity influx increase ΔS_{RF}, occur during the pulse. MIST is then run iteratively, by progressively incrementing the temperature step and decreasing the influx until the model matches the measured C V emission map and the evolution of the central chord C V and O VI normalized intensities and of their ratio. In modelling the ratio we assumed, as mentioned before, that the relative flux increases are the same for C and O. The T_{e} profile is determined by matching the computed and measured C V emission. Convergence in this procedure is possible because the emissivity dependence on ΔT_{e} is strongly nonlinear through the ionization and excitation processes, whereas ΔS dependence is nearly linear.

The computed signals again indicate fair agreement with the experiment (figure 5). The estimated temperature evolution shows a nearly 50% increase in the core temperature during the RF pulse. The absolute magnitude of the increase depends on the assumed pre-RF temperature; its relative value is nevertheless about the same for the whole range of CDX-U core temperatures.

A direct experimental check of our method, and implicitly a confirmation of the relative influx increase assumption, was obtained by comparison with Thomson scattering measurements of the core temperature in successive ohmic and (weakly) RF heated discharges. A sample of such data is presented in figure 6. We increase the accuracy of the Thomson

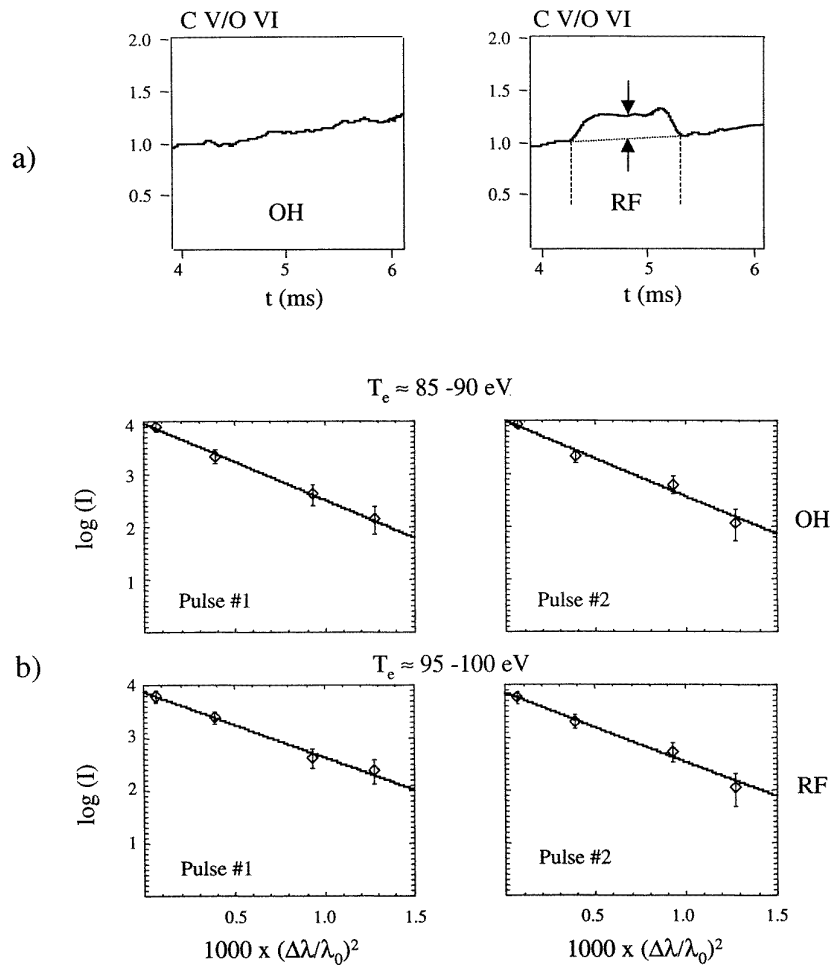

Figure 6. Example of Thomson scattering and spectroscopic data used for an experimental check of the C V/O VI technique. At least two sets of scattering data (pulse 1 and pulse 2) are obtained in each shot.

scattering estimate by using the multipulse capability of our system (up to three pulses, ≈150 μs apart, per shot) and by averaging over several reproducible discharges. We used non-sawtoothing shots, in which the temperature on axis is essentially constant around the current peak. Resulting from figures 6 and 3, the ≈25% increase in the C V/O VI ratio corresponds to an ≈10 eV core temperature increase, in good agreement with the laser measurement. (A direct read-out of the approximate temperature increase from figure 3 is acceptable in this case, since the changes in the ionization balance can be neglected for small T_e increases.) However, Thomson scattering was not available for the discharges showing strong core heating.

Finally, additional indications of core heating come from the transient change in MHD activity observed during the RF pulse. Figure 7 compares the C V signals and their frequency spectra during the pulse, with those obtained during the same interval in the OH discharge.

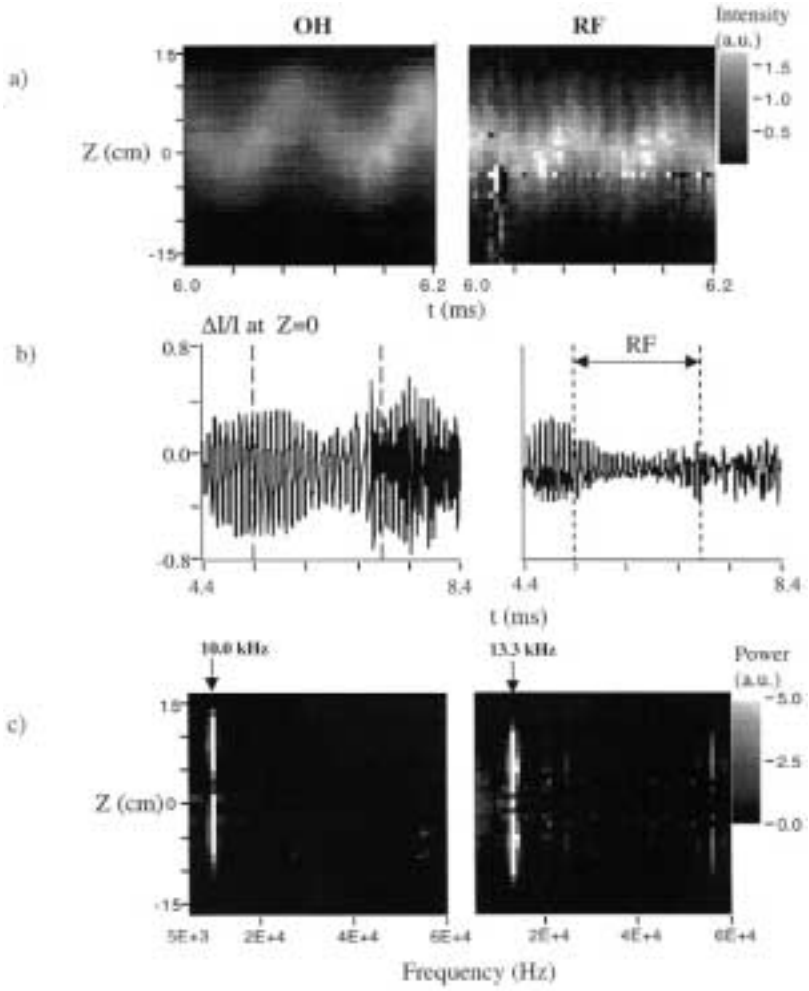

Figure 7. MHD activity characteristics in the OH and RF discharges during the time corresponding to the RF pulse: (a) intensity plot of the $m = 1$ 'snake'; (b) normalized fluctuation amplitude of the central-chord C v signal; (c) intensity plot of the power spectrum of the C v emission.

The two intense peaks at low frequency are due to the $m = 1$ 'snake'. A significant increase in the 'snake' frequency occurs during the RF pulse, from ≈10.0 kHz to ≈13.3 kHz. As in other tokamaks, the CDX-U 'snake' is found to rotate in the electron diamagnetic drift direction with approximately the perpendicular electron drift frequency at the $q = 1$ surface [17]. Indeed, using the computed profiles we estimate an approximately 30% increase in the electron drift frequency at $r/a \approx 0.5$. In addition, the amplitude of the $m = 1$ oscillation is significantly reduced compared to the OH discharge, both with regard to its relative (normalized to the instantaneous dc component) and absolute value. The relative reduction confirms that the heating is peaked on the plasma axis (the core emission is enhanced with respect to that of the $m = 1$ 'snake'), while the absolute decrease indicates an overall quench of the MHD activity, possibly caused by a change in the resistivity and current profile.

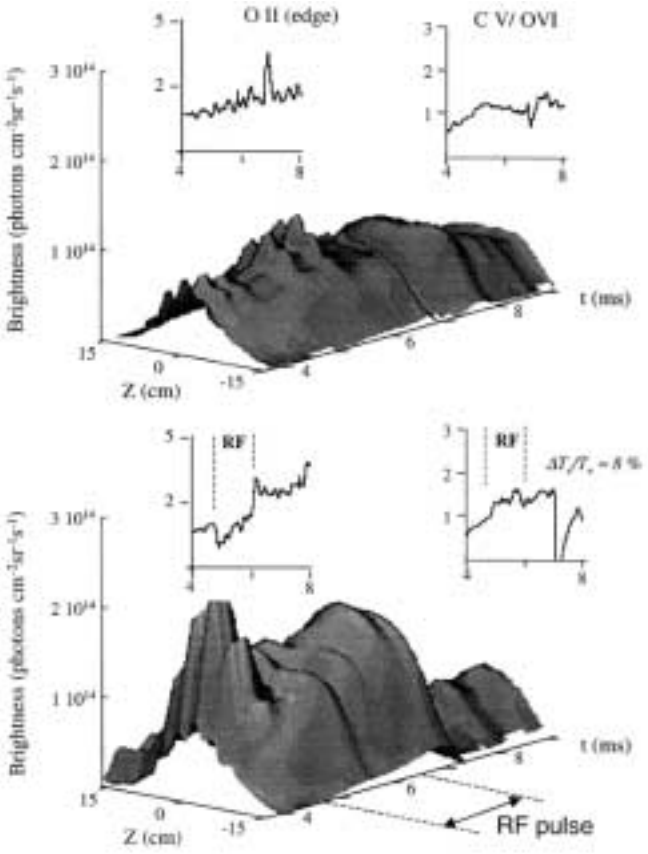

Figure 8. Spectroscopic data for ohmic and RF discharges in which significant RF heating is only indicated for the outer plasma.

Another interesting observation is the appearance during the RF pulse of (weak) fluctuations at significantly higher frequency (around 55 kHz). Their amplitude also peaks around the radius of the $q = 1$ surface. The bandwidth of the diode array is, however, insufficient for an analysis of the structure of this mode.

Strong core heating is nevertheless infrequently observed. The more typical behaviour is illustrated in figure 8. The ohmic plasma is characterized by flat C v emission profiles, that we estimate as before to be associated with flat, or slightly hollow temperature profiles. During the RF pulse although the overall core emission increases, the profiles remain flat. Both discharges exhibit steady $m = 1/m = 2$ activity, with the snake emission being enhanced during and after the RF pulse, but showing no significant change in frequency. In many discharges there are also indications of a second $m = 1$ 'snake', suggesting a non-monotonic q profile, with $q(0) > 1$.

The spectroscopic method as well as Thomson scattering, when available, indicate only a modest core heating effect, $\Delta T_{\mathrm{e\,RF}} \leqslant 10$ eV (see also figure 6). At the same time, electron temperature increases of ≈10–20 eV are routinely measured outside $r/a \approx 0.5$ using the triple Langmuir probe, with only minor density increases [3]. The MIST simulation also indicates

that the strong dip in the O II emission seen in figure 8 is consistent with a burn-through of the lower charge states in conditions of significant heating of the outer plasma and negligible impurity influx.

3. Discussion

The weak core heating is inconsistent with the ray tracing calculations, which predict the power deposition to be peaked on the discharge axis [3]. We propose an explanation for this effect, based on a parallel with the neoclassical accumulative instability recently described by Tokar *et al*, for high-Z impurities in large tokamaks [18]. Tokar and co-workers show that in the high confinement regimes in large tokamaks the high-Z impurity accumulation has the attributes of a saturated instability. The premises for this instability are: (i) the impurity transport decreases to neoclassical levels, making the neoclassical behaviour of the convective velocity important; (ii) the impurities are in the Pfirsch–Schlutter collisionality regime; and (iii) the impurity ions are incompletely stripped in the core, being able to radiate a significant fraction of the heating power.

A first consequence of the instability is that flat or hollow temperature profiles can develop above a critical electron or impurity density. Once formed, such profiles become *resilient* against auxiliary heating. The latter effect happens because, up to a certain power threshold, the additional power is radiated away by additional impurities accumulating in the core. Only above this threshold can the accumulation chain be broken and the core temperature increase. Finally, the accumulation suppresses the sawteeth giving birth to a prominent $m = 1$ 'snake' instead and eventually raises $q(0)$ above unity as a consequence of the increased resistivity on the axis.

We observe that in a low-field, low-power device like CDX-U, the conditions exist for a similar instability, involving low-Z impurities instead of high-Z ones. Indeed, since the neoclassical transport coefficients scale as $1/B_{\mathrm{T}}^2$, at fields of the order of 1 kG they may become comparable to the anomalous values. For example, the Alcator-C scaling for impurity transport predicts an O VI diffusion coefficient in CDX-U close to the estimated neoclassical value [19]. Second, as already mentioned, core ions like O VI and C V are deep in the Pfirsch–Schluter collisionality regime in CDX-U. Finally, the fast radial transport allows strongly radiating charge states like O V and O VI to emit from regions of relatively high electron temperature, which makes for a large radiative cooling coefficient [20].

Applying then the instability criterion from [18] expressed as a critical impurity concentration on the axis, we obtain for the typical CDX-U parameters

$$\left[\frac{n_{\mathrm{I}0}}{n_0}\right]_{\mathrm{crit}} \approx 2.5\times 10^{-19}\,\frac{A_{\mathrm{i}}^{1/2}}{A_{\mathrm{I}}}\,\frac{T_0^{1/2}}{L_{\mathrm{I}}}\,\frac{q_0^2}{a^2}\,\frac{Z_{\mathrm{I}}}{B_{\mathrm{T}}^2}\left(\frac{D_\perp}{D_{\mathrm{neo}}^{\mathrm{PS}}}\right)^2 \approx (3\text{–}4)\times 10^{-2}\left(\frac{D_\perp}{D_{\mathrm{neo}}^{\mathrm{PS}}}\right)^2 \qquad (2)$$

with A_{i}, A_{I} atomic weights of working and impurity ions, respectively, T_{i} in keV and the radiative cooling coefficient, L_{I} in keV m^3 s^{-1}. As in [18] and also consistent with the estimated CDX-U energy confinement time [3], we assumed a heat conductivity $\kappa_{\mathrm{e}} \approx 3n_{\mathrm{e}}D_\perp$. For the numerical estimate we used the non-equilibrium cooling coefficient for oxygen corresponding to the estimated $n_{\mathrm{e}}\tau_{\mathrm{I}}$ product in CDX-U, $L_{\mathrm{I}} \approx 6\times 10^{-16}$ keV m^3 s^{-1} [20]. Having an average oxygen concentration in this range, and with $D_\perp$ comparable to $D_{\mathrm{neo}}^{\mathrm{PS}}$, the CDX-U plasma is, therefore, prone to accumulation instability.

A direct proof of impurity accumulation cannot be reliably obtained from the C V profile, due to the high temperature sensitivity of the emission. Many other experimental observations are nevertheless consistent with the instability picture: the persistence of flat or hollow

temperature profiles, the resilience of these profiles to auxiliary heating and the increase in radiated power during RF application without any significant external impurity influx.

In addition, this mechanism would also explain the strong tendency to $m = 1$ 'snake' formation in CDX-U, the snake persistence, as well as the eventual increase of $q(0)$ above unity [18]. Finally, an earlier, unexplained observation that very distinct MHD and confinement regimes ($m = 1$ 'snake' with $T_{e0} \approx 65$ eV and sawteeth with $T_{e0} \approx 140$ eV) were obtained with only a slight change of the initial vertical field [4], may also be interpreted in terms of switching this instability by a small change in the initial impurity content.

The existence of a power deposition threshold P_{crit}, for instability suppression and for core temperature increases would also explain the infrequent heating, despite evidence of HHFW presence in the CDX-U core [3]. Indeed, applying the criterion in [18] with CDX-U parameters, and estimating the radiated power with the oxygen concentration and cooling coefficient we obtain $P_{crit} \approx 0.9$–1 W cm^{-3}. Since the ohmic deposition in the core is around 0.5–0.6 W cm^{-3}, it is seen that 'breaking-through' the saturated instability would require auxiliary power deposition comparable to the ohmic input ($\approx$150 kW), and that the $\approx$100 kW input only marginally satisfies this condition.

Finally, the differences between the estimated temperature profile evolution in the reference ohmic discharges in figures 2 and 8 also become meaningful in the light of this mechanism. The tendency to spontaneous peaking in figure 2 as compared to the steady, flat or hollow profiles in figure 8 can be explained by the CDX-U plasma being right at the threshold of the accumulation instability. In this case a slight perturbation can trigger a transition from a hollow to a peaked temperature profile on the impurity transport time scale of $\approx$1.5 ms. The strong temperature increase estimated for the RF discharge in figure 2 would then represent a synergetic effect between the RF power deposition and the spontaneous accumulation 'break-through'.

4. Summary

The spectroscopic signals offer evidence of substantial core HHFW heating in several CDX-U discharges. This conclusion results both from modelling the individual C V and O VI time histories and from the experimental confirmation of the C V/O VI ratio as a valid monitor of temperature changes in the CDX-U core. The absence of significant core heating in the majority of the discharges despite the predicted peaked RF power deposition profile, is tentatively explained through a low-Z impurity accumulation instability associated with neoclassical transport. Although a direct measure of the accumulation cannot be obtained from the available data, most of the experimental observations as well as numerical estimates are consistent with this picture. The low-Z, neoclassical accumulation mechanism may also be relevant for the start-up phase of the larger ST soon to be operated. Detailed impurity transport measurements are planned after a significant upgrade of the CDX-U capabilities. Given the relatively modest confinement properties of the target plasma, our results appear to indicate that efficient coupling of HHFW power is possible in a ST. Finally, we note that this simple method for fast and continuous diagnostics of temperature changes may be of value for other experiments if an appropriate pair of emitting ions can be found or injected into the plasma.

Acknowledgments

This work was supported by DOE grant No DE-FG02-86ER52314AT at Johns Hopkins University and DOE contract No DE-AC02-76-CHO-3703 at PPPL.

References

[1] Peng Y-K M *et al* 1996 *Fusion Technol.* **29** 210
[2] Ono M 1995 *Phys. Plasmas* **2** 4075
[3] Menard J *et al* 1999 *Phys. Plasmas* **9** 2002
[4] Ono M *et al* 1997 *PPPL Rep.* **3225** 1997
[5] Stutman D, Hwang Y S, Ono M, Finkenthal M and Moos H W 1995 *J. Electron Spectrosc. Rel. Phenom.* **78** 249
[6] Stutman D, Finkenthal M, Soukhanovskii V, May M J, Moos H W and Kaita R 1999 *Rev. Sci. Instrum.* **70** 572
[7] Huang L K, Regan S P, Finkenthal M and Moos H W 1992 *Rev. Sci. Instrum.* **63** 5171
[8] Korde R and Canfield L R 1989 *SPIE Proc.* **1140** 126
[9] Boivin R L, Goetz J A, Marmar E S, Rice J E and Terry J L 1999 *Rev. Sci. Instrum.* **70** 260
[10] Stutman D *et al* 1997 *Rev. Sci. Instrum.* **68** 689
[11] Buttery R J *et al* 1996 *Proc. 23rd EPS Conf. on Controlled Fusion and Plasma Physics (Kiev 1996)* vol 20C (Geneva: EPS) part I, p a136
[12] Hulse R A 1983 *Nucl. Technol. Sci.* **3** 259
[13] Artsimovich L A 1972 *Nucl. Fusion* **12** 215
[14] Wenzel K W and Sigmar D J 1990 *Nucl. Fusion* **30** 1117
[15] Cunningham G 1997 *Plasma Phys. Control. Fusion* **39** 1339
[16] Stangeby P S and McCracken G M 1990 *Nucl. Fusion* **30** 1225
[17] Kluber O *et al* 1991 *Nucl. Fusion* **31** 907
[18] Tokar M Z *et al* 1997 *Nucl. Fusion* **37** 1691
[19] Marmar E S, Rice J E, Terry J L and Seguin F H 1982 *Nucl. Fusion* **22** 1567
[20] Carolan P G and Piotrowicz V A 1983 *Plasma Phys. Control. Fusion* **25** 1065